Iron Oxide Nanoparticle-Mediated Development of Cellular Gap Junction Crosstalk to Improve Mesenchymal Stem Cells' Therapeutic Efficacy for Myocardial Infarction

Jin Han,[†,#] Bokyoung Kim,[‡,#] Jung-Youn Shin,[†] Seungmi Ryu,[§] Myungkyung Noh,[†] Jongsu Woo,[‡] Jin-Sil Park,[‡] Youjin Lee,[†,∥] Nohyun Lee,[⊥] Taeghwan Hyeon,[†,∥] Donghoon Choi,[*,‡] and Byung-Soo Kim[*,†,§]

[†]School of Chemical and Biological Engineering, Seoul National University, Seoul 151-744, Republic of Korea, [‡]Severance Integrative Research Institute for Cerebral & Cardiovascular Diseases, Yonsei University Health System, Seoul 120-752, Republic of Korea, [§]Interdisciplinary Program of Bioengineering, Seoul National University, Seoul 151-744, Republic of Korea, [∥]Center for Nanoparticle Research, Institute for Basic Science (IBS), Seoul 151-744, Republic of Korea, and [⊥]School of Advanced Materials Engineering, Kookmin University, Seoul 136-702, Republic of Korea. [#]These authors (J.H. and B.K.) contributed equally to this work.

ABSTRACT Electrophysiological phenotype development and paracrine action of mesenchymal stem cells (MSCs) are the critical factors that determine the therapeutic efficacy of MSCs for myocardial infarction (MI). In such respect, coculture of MSCs with cardiac cells has windowed a platform for cardiac priming of MSCs. Particularly, active gap junctional crosstalk of MSCs with cardiac cells in coculture has been known to play a major role in the MSC modification through coculture. Here, we report that iron oxide nanoparticles (IONPs) significantly augment the expression of connexin 43 (Cx43), a gap junction protein, of cardiomyoblasts (H9C2), which would be critical for gap junctional communication with MSCs in coculture for the generation of therapeutic potential-improved MSCs. MSCs cocultured with IONP-harboring H9C2 (cocultured MSCs: cMSCs) showed active cellular crosstalk with H9C2 and displayed significantly higher levels of electrophysiological cardiac biomarkers and a cardiac repair-favorable paracrine profile, both of which are responsible for MI repair. Accordingly, significantly improved animal survival and heart function were observed upon cMSC injection into rat MI models compared with the injection of unmodified MSCs. The present study highlights an application of IONPs in developing gap junctional crosstalk among the cells and generating cMSCs that exceeds the reparative potentials of conventional MSCs. On the basis of our finding, the potential application of IONPs can be extended in cell biology and stem cell-based therapies.

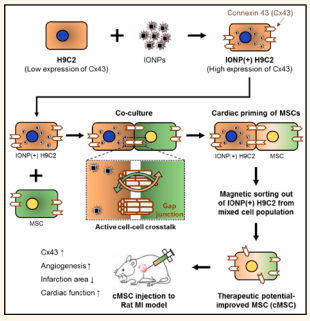

KEYWORDS: ion delivery · iron oxide nanoparticle · mesenchymal stem cells · myocardial infarction · tissue engineering

Mesenchymal stem cells (MSCs) can repair myocardium damaged by myocardial infarction (MI).[1−3] There are largely two mechanisms of action for the repair; one mechanism suggesting MSCs directly differentiate into functional cardiac cells,[4−7] and the second mechanism addressing MSCs secrete therapeutic paracrine molecules.[7−9] Although the multipotency of MSCs is promising, their cardiac differentiation *in vivo* is controversial,[1,10,11] and the lack of cardiac phenotypes in naïve MSCs poses an electrophysiological challenge for MI repair.[12−15] Previous studies have showed that MSCs expressing cardiac-specific biomarkers can reduce arrhythmic risks and improve cardiac function *in vivo*,[16−18] suggesting that cardiac phenotype development of MSCs can improve the therapeutic efficacy. Along with the cardiac phenotypes, the salutary effects of the paracrine molecules secreted from MSCs have been demonstrated in a number of studies,[19−21] and the enhanced paracrine secretion resulted in better reparative efficacy of the MSC therapies.[22−24] Hence, both cardiac phenotype development for myocardium compatibility and paracrine signaling improvements may improve the therapeutic potential of MSCs for MI.

To induce cardiac phenotype development of MSCs *in vitro*, exogenous supplements, such as transforming growth factor beta 1 (TGF-β1) and 5-azacytidine (5-AZA),

* Address correspondence to cdhlyj@yuhs.ac, byungskim@snu.ac.kr.

Received for review November 26, 2014 and accepted February 17, 2015.

Published online February 17, 2015
10.1021/nn506732n

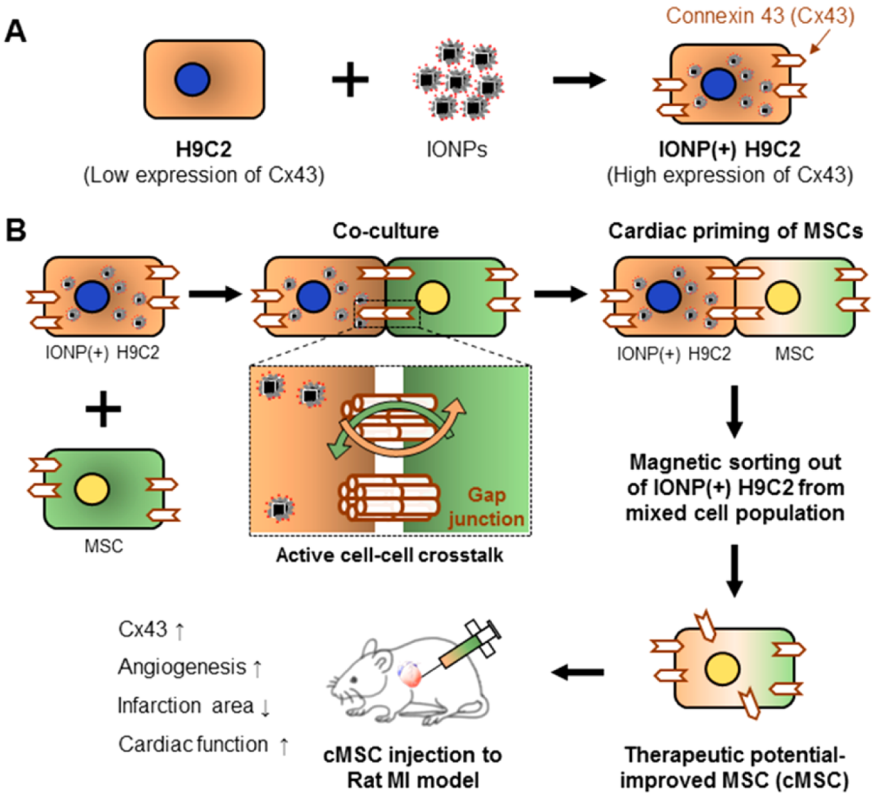

Figure 1. Schematic illustration of IONP-induced connexin 43 (Cx43) expression enhancement in H9C2, the assessments of its effects in coculture with MSCs and *in vivo* therapeutic efficacy of the cocultured MSCs. (A) Cx43 expression enhancement in H9C2 by IONP uptake. (B) Generation of therapeutic potential-improved MSCs (cMSCs) from IONP-induced active cell−cell crosstalk between IONP(+) H9C2 and MSCs in coculture, and the improved therapeutic efficacy of cMSCs *in vivo*.

have been used in MSC cultures.[25−27] Coculture with cardiomyocytes or cardiomyoblasts has also been proposed as a method for cardiac lineage differentiation that requires no exogenous supplements.[28,29] Primary cardiomyocytes, however, pose challenges for coculture, because these cells have limited life span and do not proliferate *in vitro*.[27] Moreover, the limited accessibility to the primary cardiomyocytes causes another difficulty for the coculture. To overcome these problems, cardiomyoblast cell line, H9C2, has been used in previous coculture studies.[29,30] Although H9C2 cells provide excellent accessibility and quality assurance, they rarely express connexin 43 (Cx43), a gap junction protein,[31] which is responsible for intercellular gap junction coupling and cell-to-cell crosstalk in coculture, which are previously known to play major roles in MSC modification.[17,32] Thus, H9C2 with enhanced Cx43 expression may provide active intercellular interactions with MSCs in coculture, which could promote cardiac lineage development of MSCs.

Aside from direct cardiac phenotype development of MSCs, improvement in indirect paracrine mechanism of MSCs was studied using various culture conditions. MSCs are known to repair damaged organs through a broad spectrum of reparative paracrine molecules.[11,19,20] To improve the paracrine secretion of MSCs, previous studies introduced hypoxic culture conditions or mild hypoxia generated from MSC spheroids.[22−24] Even so, no previous studies have investigated whether both cardiac phenotype development and paracrine profile improvement of MSCs could be achieved simultaneously and orchestrated into one solution for MI.

Recently, iron oxide nanoparticle (IONP)-mediated cell labeling or drug delivery has been extensively studied, and the use of IONPs in cell studies has been shown safe and effective.[33,34] In spite of their plasticity in biomedical applications, the effect of IONPs as ion-delivering carriers has rarely been studied, and their use in cell biology or stem cell-based therapy needs more exploration. While some studies have integrated IONPs to control cell behaviors *in vitro*,[35−37] approaches with IONP-induced gap junctional communication improvements have not been reported. Additionally, the mechanisms behind the nanoparticle-induced cellular behavior changes need better clarification for potential application of IONPs in the biomedical field.

In the present study, we demonstrate new biofunctional properties of IONPs in gap junctional cell−cell crosstalk and focus on the generation of therapeutic potential-improved MSCs using IONP-induced coculture with H9C2 (Figure 1). The major therapeutic mechanisms of MSC therapies for MI, namely, the

cardiac phenotype development and reparative paracrine molecule secretion, were targeted to be improved from the IONP-based coculture system. When uptaken by H9C2, IONPs are partially ionized into iron ions, which may trigger gap junctional signaling cascade to develop Cx43 expression. To address the development of Cx43 by IONPs and subsequent cellular crosstalk in coculture, we analyzed the gene and protein expression of Cx43 in IONP-harboring H9C2 (IONP(+) H9C2) and evaluated Cx43-based crosstalk of these H9C2 with MSCs in coculture. Consequently, we investigated cardiac phenotype development of MSCs influenced by Cx43-mediated cellular crosstalk in coculture with IONP(+) H9C2. Additionally, we assessed the modification of MSCs' reparative paracrine profile after coculture through gene expression and protein secretion analysis. To address the therapeutic efficacy of IONP(+) H9C2 cocultured MSCs (cMSCs), we injected cMSCs into rat MI models and evaluated cardiac tissue repair and cardiac functional recovery. Here, we demonstrate a new application of IONPs in developing cellular gap junction and propose a new window for the generation of therapeutic potential-improved MSCs from IONP-based coculture.

RESULTS AND DISCUSSION

IONP Internalization for Cell Modification. The physiological properties of iron oxide nanoparticle (IONP), and the effects of IONP-internalization in H9C2 were evaluated (Figure 2). We have utilized nanocubes rather than nanospheres to maximize the high magnetization while maintaining the colloidal stability. Since the responsiveness of IONPs to external magnetic field is proportional to their volume, larger nanoparticles are desirable for effective magnetic cell sorting. However, iron oxide nanoparticles larger than 20 nm exhibit ferromagnetic property and easily form large aggregates owing to their strong magnetic attraction to each other. Interestingly, a previous report showed that iron oxide nanocube with an edge length of 22 nm, which was encapsulated with PEG-phospholipid, exhibited high colloidal stability while maintaining high magnetization.[38] Therefore, iron oxide nanocubes with a similar size were employed in this study. The size and shape of IONP, along with the cellular uptake of nanoparticles, were assessed using transmission electron microscopy (TEM; Figure 2B). When treated with 40 μg/mL of fluorescent dye-labeled IONPs for 24 h, H9C2 showed efficient uptake of nanoparticles, and IONP clusters were observed only within the cells. IONP uptake was further visualized with a fluorescent microscope, and IONP-uptaken H9C2 (IONP(+) H9C2) expressed strong fluorescent signal compared with untreated H9C2 (IONP(−) H9C2) after 24 h (Figure 2C). To quantitatively evaluate iron contents within H9C2, both IONP(−) H9C2 and IONP(+) H9C2 were assessed with inductively coupled plasma mass spectrometry

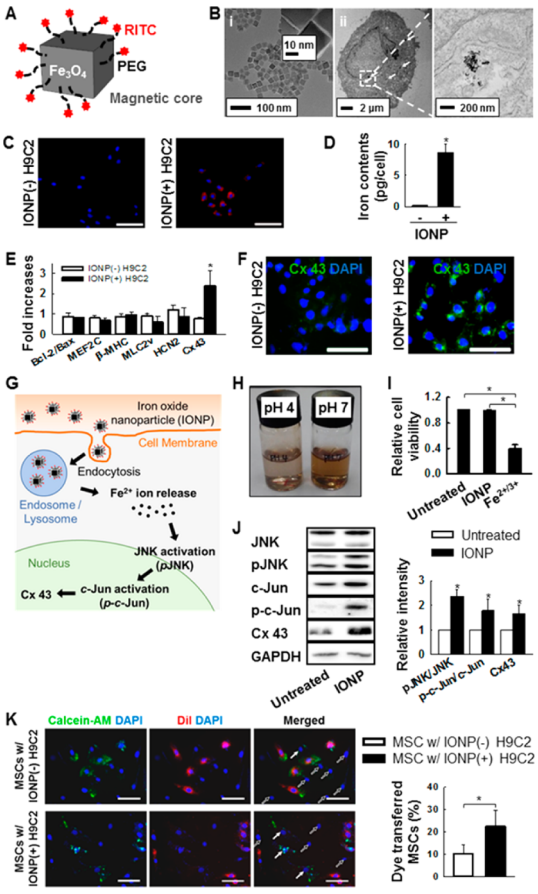

Figure 2. IONP-induced connexin 43 upregulation in H9C2 and its functional role in gap junctional crosstalk in coculture with MSCs. (A) Schematic representation of IONP. (B) TEM images of (i) IONPs (iron oxide nanoparticles) and (ii) IONPs uptaken by H9C2. IONPs are marked with white arrows. (C) Fluorescent images of H9C2 after IONP (red) treatment for 24 h. Bars, 100 μm. (D) Quantification of iron contents within H9C2 after IONP uptake. ICP-MS was performed 24 h after IONP treatment. *$P < 0.05$. (E) Expressions of H9C2-inherent cardiac and apoptosis-regulatory genes before and after IONP treatment. Gene expressions were normalized to the levels of IONP(−) H9C2. *$P < 0.05$ vs IONP(−) H9C2. (F) Expression of a gap junction protein, Cx43 (green), in H9C2 after IONP uptake. Blue indicates nuclei. Bars, 100 μm. (G) Schematic illustration of IONP-mediated signaling cascades within the cells. (H) Visualization of IONP ionization at low pH. For visualization, 40 μg/mL of IONPs were added into pH 4 or pH 7 solution, and the images were taken after 24 h. (I) The cytotoxicity of exogenous iron ions or IONPs added in H9C2 culture; 40 μg/mL of IONPs or the same molar concentration of iron ions were added directly into H9C2 culture. For cell viability evaluation, MTT assay was performed 24 h after IONP or $Fe^{2+/3+}$ treatment. *$P < 0.05$. (J) Western blot analysis and the quantification of intracellular signaling cascades for enhanced Cx43 expression triggered from IONP uptake. $n = 3$, *$P < 0.05$ vs untreated. (K) Fluorescent images and quantitative analysis showing active dye (calcein-AM, green) transfer after 48 h of coculture. Before coculture, IONP(+) H9C2 was labeled with calcein-AM and DiI (red), while MSCs were unlabeled. After 48 h of coculture, cells having green fluorescence without red (calcein-AM^+/DiI^-; solid arrow) denote MSCs that received calcein-AM through functioning gap junction. Cells having no fluorescence but DAPI (calcein-AM^-/DiI^-; hollow arrow) denote MSCs that did not receive calcein-AM during 48 h of coculture. Bars, 100 μm. *$P < 0.05$.

(ICP-MS; Figure 2D). When compared with IONP(−) H9C2, IONP(+) H9C2 showed significantly increased iron contents within the cells. Long-term residence of IONPs in H9C2 was also evaluated using TEM at 2 week time point, and sustained intracellular residence of IONPs was observed (Supporting Information Figure S1).

To evaluate whether IONP uptake affected the inherent gene expressions of H9C2, IONP(+) H9C2 were analyzed with quantitative real-time reverse transcription-polymerase chain reaction (qRT-PCR; Figure 2E). The data showed that IONP uptake did not affect the expression levels of H9C2-inherent apoptosis-regulatory (Bcl-2/BAX) or cardiac-specific genes when compared with no IONP uptake. Interestingly, IONP(+) H9C2 showed significantly improved gap junction protein connexin 43 (Cx43) gene expression compared to IONP(−) H9C2 (Figure 2E), and its protein expression was further assessed with immunocytochemistry (Figure 2F). Cellular uptake of IONPs did not affect cell viability at 2 week time point, and IONP-induced Cx43 expression was also observed at 2 week time point (Supporting Information Figure S2). The primers are listed in Supporting Information Table S1.

Next, we examined the intracellular signaling mechanisms for the improved expression of Cx43 after IONP uptake (Figure 2G). To assess the stability of IONPs at low pH, a condition that resembles cell endosomes, IONPs were added and incubated in pH 4 or pH 7 solution for 24 h. After 24 h, pH 4 solution showed better transparency compared with pH 7 solution, suggesting IONPs are partially ionized into Fe^{2+} or Fe^{3+} ions at low pH condition (Figure 2H),[39] and IONPs would generate metal ions upon endosomal uptake. Interestingly, when the same molar concentration of iron ions were directly added into the H9C2 culture, instead of using IONPs, significant cytotoxicity was observed (Figure 2I). To further evaluate the intracellular signaling cascades upon IONP uptake (Figure 2G), IONP(+) H9C2 were analyzed with Western blots (Figure 2J). When treated with IONPs, H9C2 uptake nanoparticles through endocytosis and these IONPs are retained in the intracellular endosomes.[39] Upon internalization in the endosomes, which have comparatively low pH level as low as 4,[40] IONPs are partially ionized into iron ions, and the metal ions are released into the cytosol.[39] These free metal ions promote JNK activation, c-Jun phosphorylation, and ultimately JNK-mediated Cx43 expression as expected from the previous study (Figure 2G).[41] Twenty-four hours after the IONP treatment, IONP(+) H9C2 exhibited great upregulation in the phosphorylated protein forms of JNK (*p*-JNK) and c-Jun (*p*-c-Jun) relative to the nonphosphorylated protein forms compared with untreated H9C2 (Figure 2J). Increase in *p*-JNK and *p*-c-Jun consequently activated Cx43 expression in IONP(+) H9C2.

Next, the functional role of enhanced Cx43 expression was evaluated using dye transfer assay (Figure 2K). Cx43 is known to induce intercellular coupling among the adjacent cells, and a previous study demonstrated that Cx43-overexpressing cells showed active gap junctional communication with the nearby cells and transferred biomolecules to these cells.[17] To investigate whether IONP-induced Cx43 expression in H9C2 successfully formed functional gap junctions with the adjoining MSCs and transferred cellular biomolecules, IONP(+) H9C2 or IONP(−) H9C2 were cocultured with MSCs for 48 h. Before cocultured with MSCs, both IONP(+) H9C2 and IONP(−) H9C2 were dual-labeled with DiI (red), which cannot pass through gap junctions, and calcein-AM (green), which can only pass through gap junctions. Only when H9C2 formed functional gap junctions with MSCs, calcein-AM, not DiI, would be transferred to unlabeled MSCs. When dye transfer was evaluated with fluorescence microscopy 48 h after coculture, more MSCs having calcein-AM without DiI were observed in coculture with IONP(+) H9C2 compared with the IONP(−) H9C2 coculture (Figure 2K), suggesting IONP(+) H9C2 formed more functional gap junctions with MSCs compared with IONP(−) H9C2. Quantitative analysis also showed the calcein-AM transfer from H9C2 to MSCs was significantly more frequent when H9C2 was pretreated with IONPs. This data suggests that IONP uptake can not only enhance Cx43 expression of H9C2 but also develop functional gap junction communications with MSCs in coculture.

IONP-Based Magnetic Cell Sorting after Coculture. The efficiency of IONP-assisted MSC sorting was assessed (Figure 3). Two week-cocultured cells, consisting of MSCs and IONP(+) H9C2, were trypsinized and collected in a tube and IONP(+) H9C2 were magnetized to a neodymium magnet (Figure 3A). IONP-based magnetic cell sorting induced high-density accumulation of IONP(+) H9C2 after 2 min and was evaluated with a fluorescent microscope (Figure 3B). To further assess the cell population contents, cell populations attracted to the magnet (magnet(+) population) and those not attracted to the magnet (magnet(−) population) were both stained for human nuclear antigen (HNA) to assess MSC purity (Figure 3C). HNA staining only stained human MSCs in the cell population. As shown in Figure 3C, counterstaining with 4,6-diamidino-2-phenylindole (DAPI) displayed IONP(+) H9C2 cells as $DAPI^+$ (blue)/HNA^- blue, and MSCs as $DAPI^+$/HNA^+ (green) blue-green. After magnetic cell separation, no IONP(+) H9C2 was observed in the magnet(−) population (Figure 3C). Similarly, almost no MSCs was observed in the magnet(+) population. The immunofluorescent images were then quantitatively evaluated. To further confirm pure MSC population in the magnet(−) population, the cell population for *in vivo* injection, the MSC purity was evaluated using

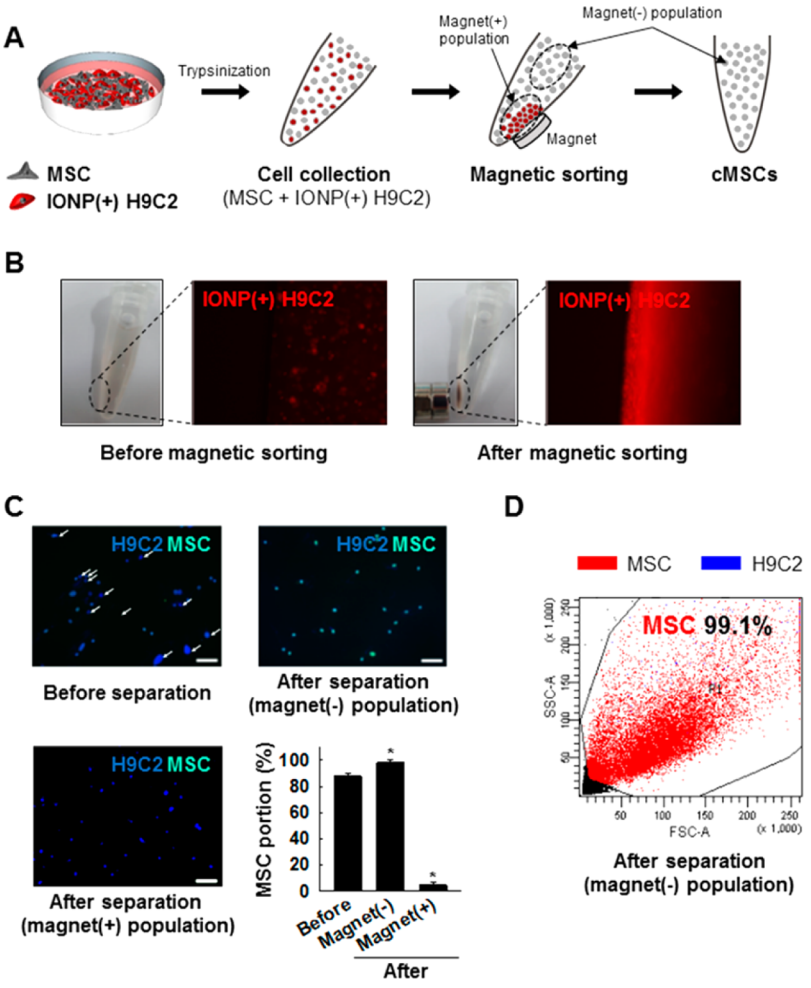

Figure 3. Facile separation of cMSCs following 2 week coculture by magnetically removing IONP-harboring H9C2 from the cocultured cell population. (A) Representative illustration of the cell sorting method. Cells attracted to the magnet (magnet(+) population) were segregated from the cells not attracted to the magnet (magnet(−) population) and discarded to leave pure cMSC population. (B) Macroscopic fluorescent visualization of IONP(+) H9C2 (red) sorting using a magnet. (C) Efficiency of IONP-induced cell sorting. $DAPI^+$ (blue)/ HNA^- H9C2 were visualized as blue, and $DAPI^+$/ HNA^+ (green) human MSCs were visualized as blue-green. Fluorescent images were taken and quantified for both magnet(−) and magnet(+) populations. H9C2 are marked with white arrows in the first image (before separation). Bars, 100 μm. *$P < 0.05$ vs before separation. (D) FACS result of the IONP-based cell sorting.

fluorescent-activated cell sorting (FACS; Figure 3D). FACS result demonstrated over 99% pure MSCs in the magnet(−) population. Facile separation of MSCs after coculture is particularly intriguing because conventional cell sorting method after coculture faces several challenges. For cardiac differentiation of MSCs or endothelial progenitor cells, direct cell-to-cell contact with cardiomyocytes or cardiomyoblasts was shown pivotal.[28,29] Even so, cell separation following coculture necessitates costly cell-specific antibodies, sorting equipment, and expertise, thereby limiting simple, efficient, and clinical-scale cell sorting. Moreover, the inability to eliminate cell-conjugated antibodies after antibody-induced cell sorting could be problematic for the transplantation of the cocultured cells. Likely for this reason, *in vivo* administration of the cocultured MSCs for MI has rarely been reported. In contrast, IONP-based coculture facilitated a simple, cost-effective, easily scalable, and efficient cell sorting following coculture, allowing for the separation of transplantable dosages of MSCs for *in vivo* applications.

Cardiac Phenotype Development of MSCs after Coculture. Cellular phenotype changes in the cocultured MSCs were evaluated by analyzing the expression of cardiac-specific biomarkers (Figure 4). MSCs were cocultured with IONP(+) H9C2 or IONP(−) H9C2 and sorted by neodymium magnet or FACS, respectively. After 7 days of coculture, MSCs cocultured with IONP(−) H9C2 showed no significant changes in their cardiac genes compared with unmodified MSCs. However, MSCs cocultured with IONP(+) H9C2 showed significant increase in cardiac-specific genes including ß-MHC, MLC2a, and MLC2v (Figure 4A). This data suggests that the improved gap junctional communication from IONP uptake (Figure 2J,K) successfully induced cardiac phenotype development of MSCs after coculture.

To further compare the cardiac phenotype development efficacy of IONP-based coculture with the

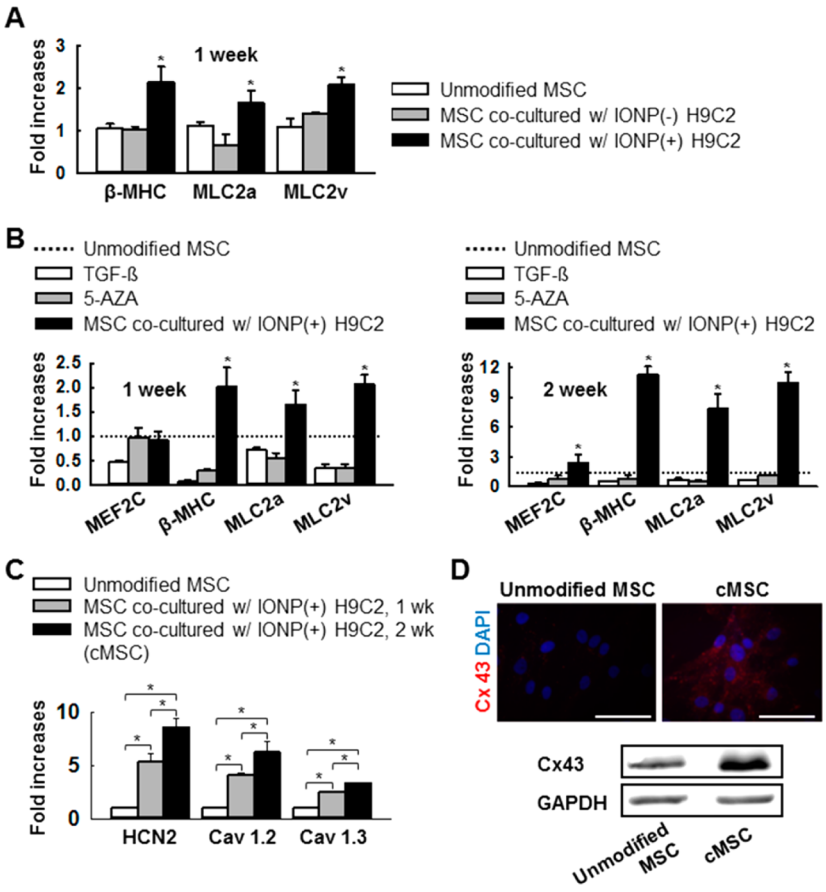

Figure 4. Effective development of cardiac phenotype in MSCs by coculture with IONP(+) H9C2. The expression levels of the genes were normalized to the levels of unmodified MSCs. (A) IONP-dependent cardiac phenotype development of MSCs. *$P < 0.05$ vs any group. (B) Enhanced cardiac phenotype development of MSCs by IONP-induced coculture compared with the conventional cardiac differentiation methods, treated with TGF-β or 5-azacytidine. *$P < 0.05$ vs any group. (C) Culture period-dependent expression of ion channel genes in cMSCs (MSCs cocultured with IONP(+) H9C2). *$P < 0.05$. (D) Immunocytochemistry staining and Western blot analysis for connexin 43. Bars, 100 μm.

conventional cardiac differentiation methods, a number of groups were analyzed with qRT-PCR (Figure 4B). After 7 and 14 days of culture, qRT-PCR was performed for unmodified MSCs, MSCs treated with cardiac differentiation supplements, such as TGF-β1 or 5-AZA, and MSCs cocultured with IONP(+) H9C2. As shown in Figure 4B, only the MSCs cocultured with IONP(+) H9C2 showed distinctively increased mRNA expression of cardiac-specific proteins compared with the other groups. Cocultured MSCs exhibited increased expression levels of a cardiac transcription factor, MEF2C, as well as the midlate cardiac structural genes β-MHC and MLC. Increase in cardiac structural gene expressions was dependent on the coculture period, and the similar tendency was observed in cardiac ion channel marker expressions (Figure 4C). A significant increase in the mRNA expression of ion channel proteins was observed in 2 week cocultured MSCs (cMSCs) compared with unmodified or 1 week cocultured MSCs (Figure 4C). On the basis of these data, the optimal coculture period needed for MSCs to develop cardiac phenotypes was set to 2 weeks. When the expression of sarcomeres was evaluated for cMSCs and unmodified MSCs, however, only a small fraction of cMSCs expressed sarcomeric α-actinin, and no expression was observed in MSCs (Supporting Information Figure S3). Immunocytochemistry and Western blot analysis were then performed to evaluate the expression of Cx43 in cMSCs compared with unmodified MSCs (Figure 4D). Cx43 expression is particularly important because Cx43 plays a critical role in gap junctional communications in the myocardium.[42,43] After acute myocardial infarction, severe loss of healthy myocardium impairs intercellular communications at the peri-infarct and induces cardiac conduction disturbances.[42−44] Administration of naïve MSCs at this phase faces compatibility issues and may pose arrhythmic risks.[13,14] Previous studies addressed that abnormal cardiac conduction and arrhythmogenic remodeling after MI could be worsened by low Cx43 expression, immature ion channel activity, or even a physiological incompatibility of naïve MSCs.[12,14,45] Interestingly, injection of MSCs expressing cardiac biomarkers or genetically modified cells that overexpress Cx43 conferred a better reparative effect post-infarct.[12,16,17] Previous studies also showed that

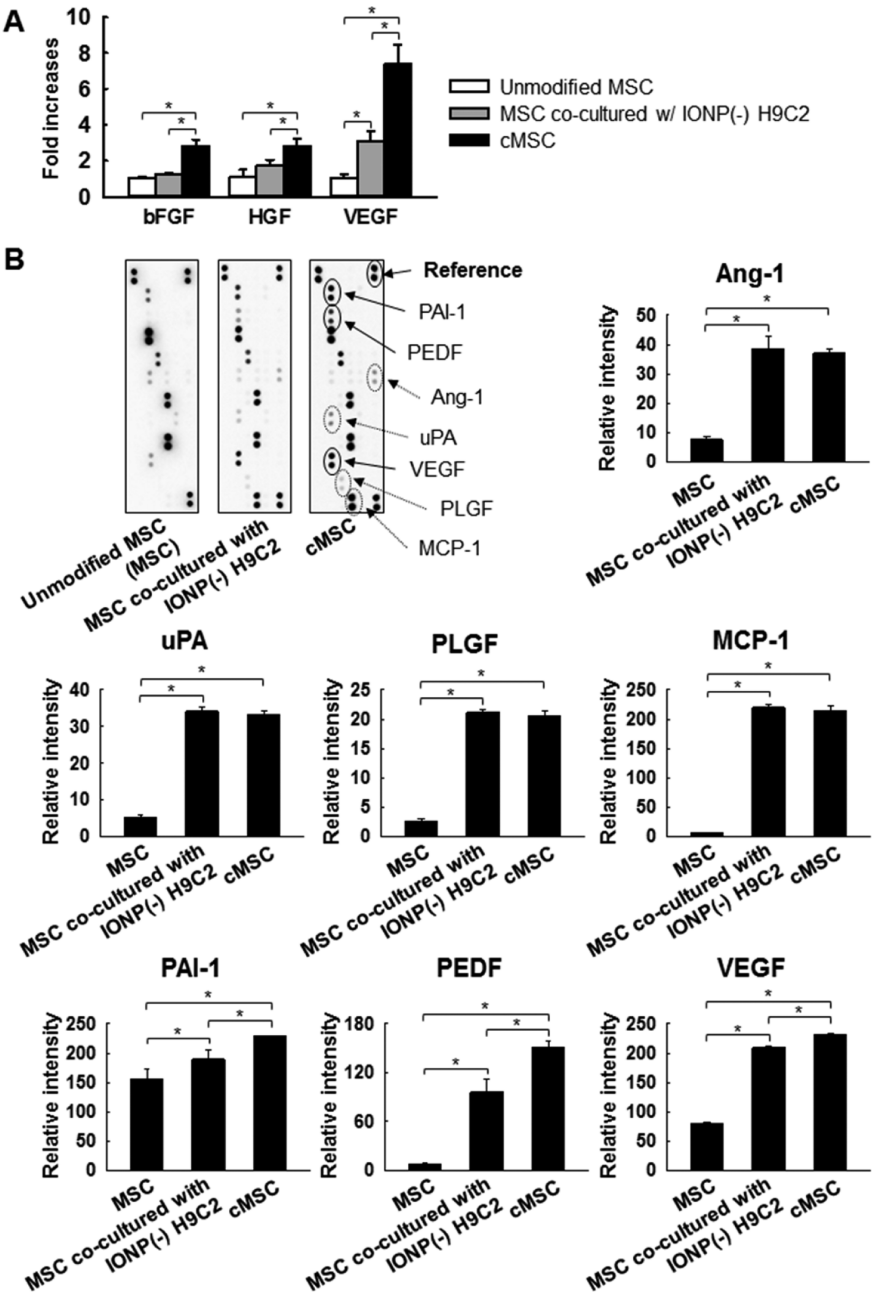

Figure 5. Cardiac repair-favorable paracrine profile of cMSCs (MSCs cocultured with IONP(+) H9C2). Expressions were normalized to the levels of unmodified MSCs. (A) Enhanced gene expressions of angiogenic proteins in MSCs, as evaluated by qRT-PCR. *$P < 0.05$. (B) Representative images and quantitative analysis of the protein array. Paracrine molecules with significant differences in pixel densities compared to unmodified MSCs or MSCs cocultured with IONP(−) H9C2 labeled with dotted or solid lines, respectively. $n = 3$, *$P < 0.05$.

overexpression of connexin 43 in MSCs or skeletal muscle cells can greatly improve the therapeutic efficacy of the cell therapy in MI regardless of the cellular arrangement of connexin 43.[12,16−18,46]

MSC overexpression of cardiac structural genes, ion channel biomarkers, and Cx43 from the IONP-based coculture could associate with enhanced therapeutic efficacy *in vivo*. A number of previous studies tried terminal cardiac differentiation of MSCs, however, developing functional cardiac behaviors such as action potential generation or calcium transient was limited.[16,17,25,26,28,32,47,48] Hence, the present study did not address action potential generation or calcium transient in MSCs. However, adaptation of electrophysiological biomarkers showed promising results in MI treatment.[16−18] Accordingly, we focused to potentiate the therapeutic efficacy of MSC therapy by addressing their electrophysiological phenotype development.

Cardiac Repair-Favorable Paracrine Profile of cMSCs. The alteration of the cellular paracrine profile in MSCs after IONP-based coculture was assessed by qRT-PCR and protein array analysis (Figure 5). Angiogenic and

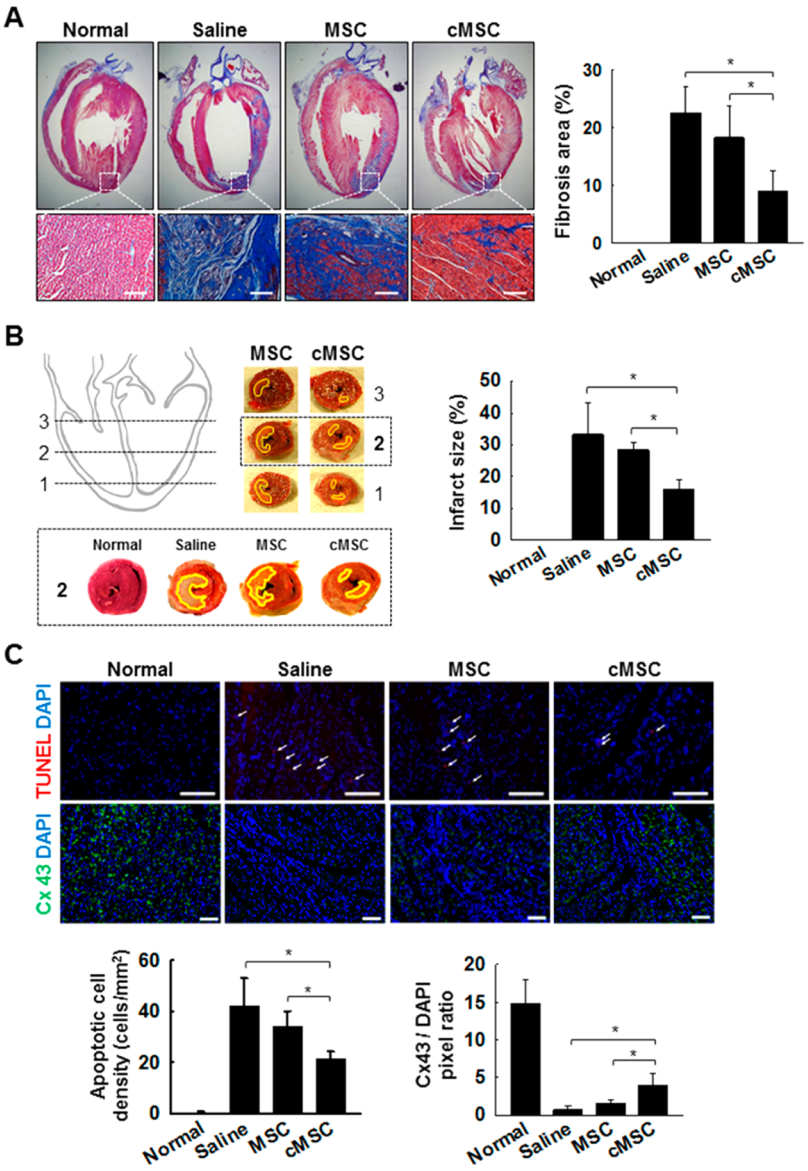

Figure 6. Injection of cMSCs attenuates left ventricular remodeling. (A) Histological sections of myocardium stained with Masson's Trichrome, and their quantitative analysis. $n = 4$ animals, $^*P < 0.05$. Bars, 200 μm. (B) Images of TTC stained heart sections, and the quantitative analysis. The infarcted area is marked with a yellow line. $n = 4$ animals, $^*P < 0.05$. (C) Immunohistochemistry images of apoptotic cells and gap junction proteins at the border zone. TUNEL$^+$ apoptotic cells (red) are marked with white arrows. Apoptotic cells were quantified as the number of TUNEL$^+$ cells per mm^2. Cx43 expression (green) was quantified using densitometry and evaluated relative to DAPI$^+$ expression. Bars, 100 μm. $n = 4$ animals, $^*P < 0.05$.

cardioprotective proteins that are inherently expressed in MSCs were first evaluated with qRT-PCR (Figure 5A). Interestingly, cMSCs exhibited augmented gene expression of angiogenic proteins such as basic fibroblast growth factor (bFGF), hepatocyte growth factor (HGF), and vascular endothelial growth factor (VEGF) compared with unmodified MSCs or MSCs cocultured with IONP(−) H9C2 (Figure 5A). bFGF and VEGF are known to promote angiogenesis and induce proliferation of endothelial cells,[3,11,22] while HGF has cytoprotective and antiapoptotic effects.[9,11] This finding is particularly interesting because coculture of MSCs with IONP(+) H9C2 affected not only the cardiac-specific gene expression (Figure 4) but also the angiogenic gene expression in MSCs. Additionally, upregulation of these therapeutic genes was IONP-dependent, suggesting that IONP-induced gap junctional coupling was critical in developing cardioprotective gene expression in MSCs during coculture.

To further evaluate the paracrine profile improvement by coculture with IONP(+) H9C2, we performed protein array analysis for the conditioned media of unmodified MSCs, MSCs cocultured with IONP(−) H9C2, and cMSCs. Cocultured MSCs were first sorted and replated to a culture plate. Initial number of the plated cells was kept the same for all groups (unmodified MSCs, MSCs cocultured with IONP(−) H9C2, and cMSCs). Figure 5B demonstrates representative

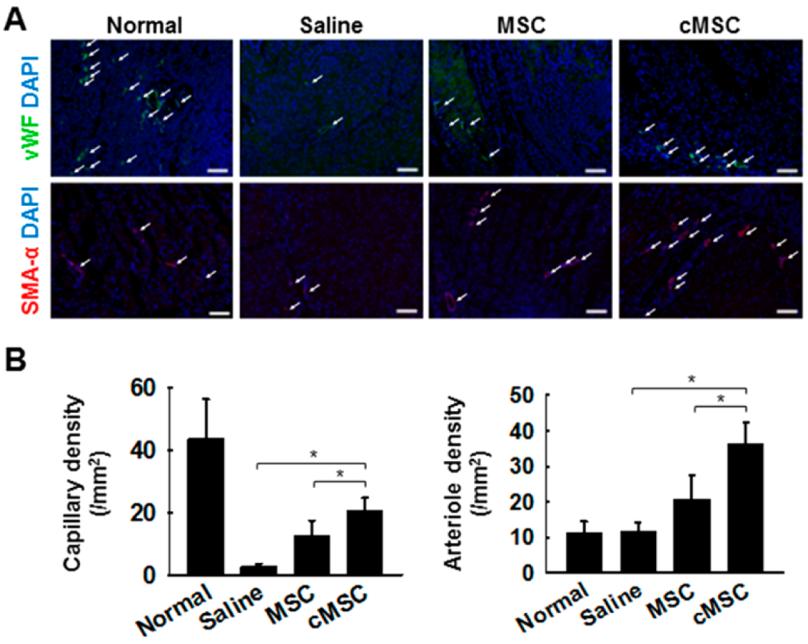

Figure 7. Injection of cMSCs increases vessel density at the peri-infarct. (A) Expression of vWF (upper images; white arrows) and SMA-α (lower images; white arrows) at the peri-infarct, 2 weeks after the treatments. Bar, 100 μm. (B) Quantification of capillary and arteriole density. Vascular densities were quantified as vWF^+ or SMA-α^+ vessels per mm^2. n = 4 animals, *$P < 0.05$.

dot blots and quantitative analysis of the assay 2 days after the MSC replating. MSCs cocultured with H9C2, regardless of their IONP uptake, produced large number of cytokines compared with unmodified MSCs. Proteins that are known to repair damaged myocardium, such as angiopoietin 1 (Ang-1) and urokinase-type plasminogen activator (uPA) that reduce infarct size,[49−51] along with placental growth factor (PlGF) and monocyte chemoattractant protein-1 (MCP-1) that help collateral perfusion,[52] showed significant upregulation in both MSCs cocultured with IONP(−) H9C2 and cMSCs compared with unmodified MSCs. Surprisingly, the secretion of plasminogen activator inhibitor-1 (PAI-1), pigment epithelium-derived factor (PEDF), and VEGF was shown IONP-dependent and was significantly increased in cMSCs compared to MSCs cocultured with IONP(−) H9C2. PAI-1 is known to promote angiogenesis by stimulating endothelial cell migration[53] and is expected to protect damaged myocardium from extensive fibrosis.[54] Also, PEDF and VEGF have been suggested to have a protective role in MI and reduce collagen deposition for improved cardiac function, respectively.[55,56] After magnetic cell sorting, cMSCs remained active for 1 week to secrete the paracrine molecules (PLGF, MCP-1, PEDF, and VEGF) and showed increased cytokine secretion compared to unmodified MSCs (Supporting Information Figure S4). This suggests that the enhancement in paracrine profile was not transient. Upregulation in paracrine molecules is beneficial in myocardium regeneration, as a number of studies has previously emphasized the reparative and long-term effect of paracrine signaling of MSCs.[57−59] Our study demonstrates that cMSCs show higher levels of therapeutic gene expression and protein secretion compared with unmodified MSCs or MSCs cocultured with IONP(−) H9C2. Although we could not specify which type of molecules were transferred from H9C2 to MSCs, IONP-dependent developments of therapeutic gene expression and paracrine profile were clearly demonstrated. Significant enhancements in MSC's innate cytokine profile could augment the therapeutic efficacy of stem cell therapy.[17]

Left Ventricular Remodeling Attenuation *in Vivo*. Attenuation of ventricular remodeling by cMSC administration *in vivo* was assessed (Figure 6). Rats were treated with no operation as a positive control, with saline as a negative control, with MSCs as a conventional MI treatment, and with cMSCs as the experimental group. Two weeks after the treatments, Masson's trichrome staining was performed to assess the area of collagen-containing fibrous tissue. Longitudinal sections of the heart showed markedly low levels of blue-colored fibrotic tissue area in the cMSC group (Figure 6A). Quantitative analysis showed that the injection of cMSCs significantly reduced fibrotic tissue formation compared with the injection of saline or MSCs (8.9 ± 3.6 *versus* 22.6 ± 4.5 and 18.2 ± 5.6%, respectively; $P < 0.05$). The administration of cMSCs was also associated with superior infarct size suppression (Figure 6B). Infarct size was analyzed by triphenyl tetrazolium chloride (TTC) staining and quantitatively assessed by measuring the ratio of infarcted myocardium in the left ventricle. The degree of infarct size was significantly lower in the cMSC group compared with

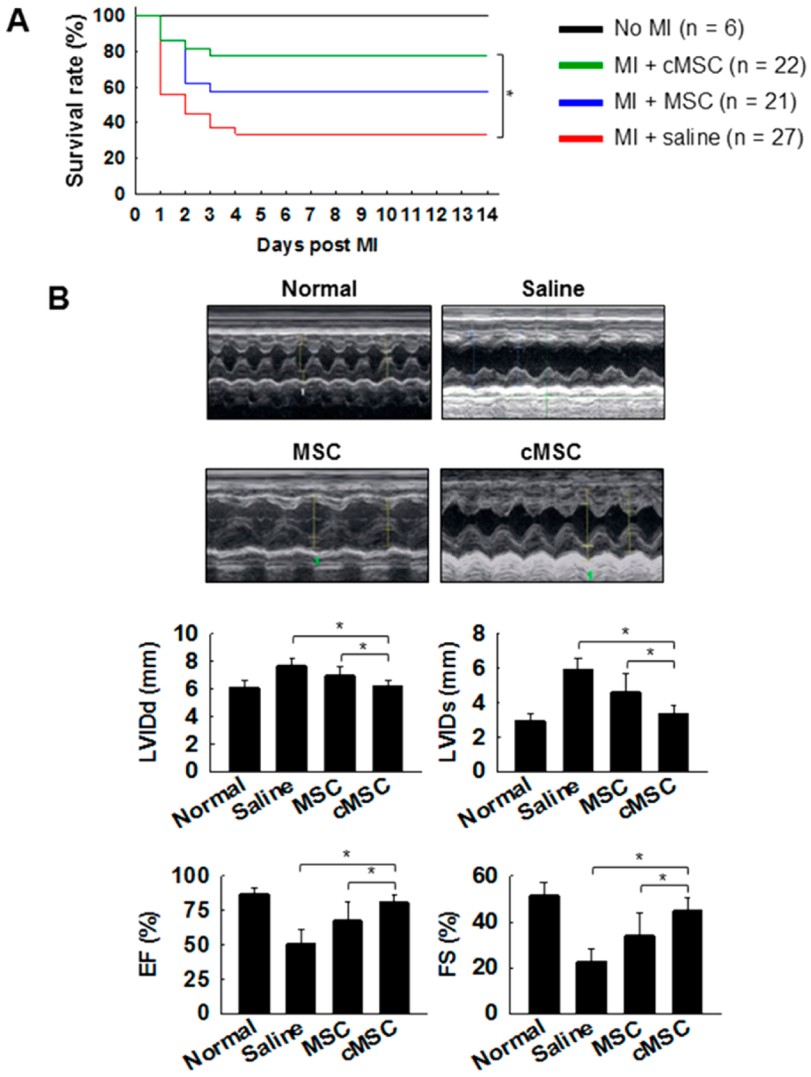

Figure 8. Injection of cMSCs improves animal survival and cardiac functions. (A) The cumulative animal survival rate. *$P < 0.05$, log-rank analysis. (B) Representative images and the quantitative analysis of echocardiography. $n = 6$ animals, *$P < 0.05$.

the saline or MSC groups (15.7 ± 3.2 *versus* 33.0 ± 9.9 and 28.2 ± 2.6%, respectively; $P < 0.05$).

Regulation of cardiac remodeling was further assessed with myocardium apoptosis and endogenous gap junction protein expression (Figure 6C). ApopTag Fluorescein *In Situ* Apoptosis Detection Kit (TUNEL) assay and immunohistochemistry for Cx43 were performed 2 weeks after the treatments. The administration of cMSCs decreased peri-infarct apoptotic cell numbers compared with the injection of saline or MSCs (20.9 ± 3.2 *versus* 41.9 ± 11.1 and 33.9 ± 6.2 cells/mm^2, respectively; $P < 0.05$). Consequently, the densitometry ratio of Cx43 to DAPI at the peri-infarct was higher in the cMSC group compared with the saline or MSC groups (3.9 ± 1.6 *versus* 0.6 ± 0.5 and 1.4 ± 0.5, respectively; $P < 0.05$). This data suggests that cMSC injection salvaged dying cardiac cells and better preserved Cx43 expression.

Increased Vessel Density *in Vivo*. To confirm that the increased vascular growth was involved with the improvement in cardiac remodeling, the heart sections were stained 2 weeks after the treatments for the expression of von Willebrand Factor (vWF) and smooth muscle actin alpha (SMA-α) (Figure 7). Capillary density was notably higher in the cMSC group compared with the saline or MSC groups (20.3 ± 4.3 *versus* 2.6 ± 0.9 and 12.3 ± 5.1 vessels/mm^2, respectively; $P < 0.05$). The cMSC group also showed higher arteriole density at the border zone compared with the saline or MSC groups (36.3 ± 6.2 *versus* 11.7 ± 2.6 and 20.8 ± 6.8 vessels/mm^2, respectively; $P < 0.05$). Our observations demonstrate that the suppression of physiological remodeling of the heart was accompanied by enhanced capillary and arteriole growth.

Animal Survival and Cardiac Function Improvements. Improvements in animal survival and cardiac function after cMSC injection were evaluated (Figure 8). The cumulative animal survival rate was analyzed with Kaplan–Meier analysis ($n = 6$ animals for normal, 27 for saline, 21 for MSC, and 22 for cMSC; Figure 8A).

The cMSC group displayed the highest animal survival compared with the other groups. The MSC group showed an increase in survival, but not significant, compared with the saline group ($P > 0.05$). The cMSC group, however, showed a significant increase in animal survival compared with the saline group ($P < 0.05$). Interestingly, a notable change in animal survival was detected only within 72 h after treatment. Previous studies showed the ventricular arrhythmias are most likely observed within 48−72 h after infarction, and they can be regulated with increased expression of cardiac ion channel genes and gap junction protein of the injected cells.[12,14,60] Thus, the improved survival in cMSC-treated animals at the initial phase of MI could have been mediated by the cardiac electrophysiological properties of cMSCs.

To further investigate the functional recovery of the ischemic myocardium, transthoracic echocardiography was performed and quantified (Figure 8B). Two weeks after the treatments, both left ventricular internal diameter at end diastole (LVIDd) and at end systole (LVIDs) were markedly decreased in the cMSC group (LVIDd = 6.2 ± 0.5; LVIDs = 3.4 ± 0.5 mm) compared with the saline (7.6 ± 0.6; 5.9 ± 0.7 mm; $P < 0.05$) or MSC (7.0 ± 0.7; 4.6 ± 1.1 mm; $P < 0.05$) groups. The improvements in LVIDd and LVIDs collectively affected the contractility of the heart and greatly recovered the ejection fraction (EF) ratio and fractional shortening (FS) in the cMSC group (EF = 80.3 ± 5.9; FS = 44.7 ± 5.7%) compared with the saline (50.9 ± 10.4; 22.6 ± 5.7%; $P < 0.05$) or MSC (67.4 ± 14.2; 34.0 ± 10.2%; $P < 0.05$) groups (Figure 8B). A previous study has shown that MSCs that express cardiac biomarkers can reduce early animal sudden death, and MSCs' paracrine signaling results in prolonged myocardium protection.[16] We expect the developments of cardiac phenotype and reparative paracrine profile in cMSCs from the IONP-based coculture functioned cooperatively to prevent physiological remodeling of the heart and resulted in cardiac function recovery.[16,23,61]

Long-term engraftment of MSCs, however, was not observed in this study, conforming to the previous studies that showed improved cardiac function with insignificant long-term survival of the injected MSCs (Supporting Information Table S2).[62−66] Injection of human-derived MSCs into rat models could have attributed to the low MSC survival, but a previous study also reported that allogenic injection of rat MSCs also showed rapid cell clearance with improved cardiac function.[62,65,67] Even so, the physiological properties of cMSCs that were previously known to be beneficiary for MI treatment, including connexin 43 overexpression (Figure 4),[12,18,46] cardiac electrophysiological gene expression (Figure 4),[13,14,16] and paracrine signaling (Figure 5),[7−9,22,68] contributed to the remarkable improvement in cardiac tissue repair and function.

CONCLUSIONS

In this study, we demonstrate a novel approach of utilizing IONPs for cellular gap junction development, and the generation of therapeutic potential-improved cMSCs through coculture with IONP-harboring H9C2. IONP uptake by H9C2 triggered intracellular signaling cascade, which subsequently enabled gap junctional coupling of H9C2 with MSCs and active cellular crosstalk in coculture. MSCs cocultured with IONP(+) H9C2 showed enhanced therapeutic properties, namely, a cardiac phenotype development, which may reduce electrophysiological challenges of naïve MSCs, and a unique paracrine profile, which provides more cardiac repair-favorable cytokines. Injection of cMSCs with cardiac phenotype and improved cytokine profile into rat MI models significantly improved cardiac tissue repair and functional recovery. The IONP-based coculture platform can be used to potentiate the therapeutic efficacy of MSCs for MI.

METHODS

Preparation of IONPs. Iron(III) acetylacetonate (0.706 g, Acros, 99%) was dissolved in benzyl ether (10.40 g, Aldrich, 99%) solution containing oleic acid (1.27 g, Aldrich, 90%) and 4-phenylcarboxylic acid (0.4 g, Acros, 95%). The solution was degassed under vacuum for 1 h, refilled with argon, and heated to 290 °C with a heating rate of 20 °C/min. After maintaining 290 °C for 30 min, the solution was cooled to room temperature. To precipitate the resulting nanoparticles, acetone or ethanol was added to the solution, which was centrifuged at 1700 rpm for 10 min. The separated precipitate was dispersed in nonpolar chloroform. The shape and size of the nanoparticles were confirmed using transmission electron microscope operating at 200 kV. To make the nanoparticles hydrophilic, they were then encapsulated using 1,2-distearoyl-*sn*-glycero-3-phosphoethanolamine-*N*-[methoxy(polyethylene glycol)-2000] (DSPE-mPEG) and 1,2-distearoyl-*sn*-glycero-3-phosphoethanolamine-*N*-[amino(polyethylene glycol)-2000] (DSPE-PEG-NH2, Avanti Polar Lipids, Inc., Alabaster, AL). Typically, 10 mg of DSPE-mPEG and DSPE-PEG-NH2 was added to 2 mL of IONP solution in chloroform. After evaporating the solvent, 2 mL of sterilized water was added and sonicated to disperse the nanoparticles. Excess PEGylated phospholipids were removed using ultracentifugation at 20 000 rpm for 1 h. Subsequently, aggregates or contaminants were removed using a cellulose acetate syringe filter (Advantec, Japan). To conjugate fluorescence dyes, nanoparticles with amine groups were dispersed in phosphate buffer saline. One milligram of rhodamine B isocthiocyanate (RITC) was added, and the solution was stirred for 6 h. Excess RITC was removed using a desalting column (PD-10, GE Healthcare Life Sciences, Pittsburgh, PA). The final product was analyzed using TEM.

Cell Culture and IONP Uptake. Human bone marrow MSCs were purchased from Lonza (Walkersville, MD), and rat cardiac myoblast cell line H9C2 cells were purchased from Korean Cell Line Bank (Seoul, Korea). Both MSCs and H9C2 cells were cultured in growth medium consisting of low-glucose DMEM (Gibco, NY) supplemented with 10% (v/v) FBS, 100 units/mL penicillin, and 100 μg/mL streptomycin. To prepare IONP(+) H9C2 cells, nanoparticles were added into the medium at a concentration

of 40 μg/mL. After 24 h, the cells were washed thoroughly with PBS. For the detection of internalized IONPs, the cells were analyzed using TEM and fluorescent microscopy (Model IX71, Olympus, Tokyo, Japan). The cytotoxicity of IONP was measured using MTT and qRT-PCR. Intercellular iron contents were then measured using inductively coupled plasma mass spectrometry (ICP-MS; ICPS-7500, Shimadzu, Kyoto, Japan). To compare the cytotoxicity of IONPs to direct iron ion delivery, H9C2 were treated with 40 μg/mL IONPs, or with the same molar concentration of $Fe^{2+/3+}$ in 40 μg/mL IONPs, and MTT assay was performed after 24 h. To evaluate the intracellular signaling cascade upon IONP uptake, Western blot analysis was performed.

IONP-Based Coculture of MSCs. To prepare the IONP(+) H9C2 feeder layer, H9C2 cell proliferation was first inhibited with mitomycin-C (Sigma) at a concentration of 10 μg/mL for 2 h. The cells were washed with PBS, and the media was switched to fresh growth medium. IONPs were then added into the medium. After 24 h of incubation, the cells were washed with PBS and plated at a density of 3000 cells/cm^2 in 150 mm culture dishes (total 5×10^5 cells). Two days later, 2×10^5 MSCs were seeded into the IONP(+) H9C2 cell-plated 150 mm culture dishes. A cell number ratio of 2:1 between IONP(+) H9C2 and MSCs was used in this study because, when 1:1 ratio was used for coculture, mitomycin-C-treated, nonproliferating IONP(+) H9C2 was overwhelmed by proliferative MSCs after 1 week, limiting cell−cell crosstalk. When cell number ratio of 3:1 was used, however, there were comparatively too many IONP(+) H9C2 compared to MSC, resulting in noneffective cell−cell crosstalk. To maximize cellular contacts between IONP(+) H9C2 and MSCs, we optimized the cell number ratio to 2:1 between IONP(+) H9C2 and MSCs.

For the analysis of dye transfer from H9C2 to MSCs, both IONP(+) H9C2 and IONP(−) H9C2 were prelabeled with DiI (6.25 μg/mL; Sigma) and calcein-AM (10 μmol/L; Sigma) before cocultured with MSCs. After 48 h of coculture, the cells were counterstained with DAPI, and dye transfer was evaluated using fluorescent microscope.

IONP-Driven Cell Sorting after Coculture. After 7 and 14 days of coculture, the mixture of MSCs and IONP(+) H9C2 cells were collected by trypsinization, resuspended in growth medium, and collected into Eppendorf tubes. A neodymium magnet was placed right next to the tube to induce cell sorting, while the cell suspension was continually gently mixed for dispersion. After 2 min of sorting, macroscopically dark colored IONP(+) H9C2 cells were magnetized to the magnet and accumulated at the bottom of the tube. Only the top suspension of the cells was collected and resuspended in growth medium. Magnet-induced cell sorting was repeated 5 more times. After the sixth sorting, the homogeneous MSC suspension was collected, and the purity was evaluated by immunofluorescent staining for HNA and by FACS installed at the National Center for Inter-university Research Facilities (NCIRF) at Seoul National University (FACS Aria II, Seoul, Korea).

***In Vitro* Assessments.** Upregulation in cardiac specific gene expression was measured with qRT-PCR. RNA was extracted from the cells and reverse-transcribed into cDNA. Expression of cardiac structural and ion channel genes were measured using StepOnePlus real-time PCR system (Applied Biosystems, Foster city, CA) with FAST SYBR Green PCR master mix (Applied Biosystems) for 45 cycles. Each cycle consisted of the following temperatures and times: 94 °C for 3 s and 60 °C for 30 s. The primers are listed in Supporting Information Table S1.

For protein detection, immunohistochemistry and Western blot analysis was performed against Cx43 for MSCs and 2 week-cocultured cMSCs.

For Western blot analysis, IONP(+) H9C2 lysate was prepared using sodium dodecyl-sulfate (DS) sample buffer (62.5 mM Tris-HCl (pH 6.8), 2% (w/v) SDS, 10% (v/v) glycerol, 50 mM dithiothreitol, and 0.1% (w/v) bromophenol blue). The total concentration of the protein was determined with bicinchoninic acid protein assay (Pierce Biotechnology, Rockford, IL) and further performed through 10% (w/v) SDS-polyacrylamide gel electrophoresis. Proteins were transferred to Immobilon-P membrane (Millipore Corp., Bedford, MA) and probed with antibodies against c-Jun N-terminal kinases (JNK; Abcam, Cambridge, U.K.), phosphorylated JNK (*p*-JNK; Abcam), c-Jun (Abcam), phosphorylated c-Jun (*p*-c-Jun; Abcam), connexin 43 (Cx43; Abcam). and beta actin (ß-actin; Abcam). Proteins were incubated with horseradish peroxidase-conjugated secondary antibody (Santa Cruz Biotechnology, Santa Cruz, CA) for 1 h at room temperature, and blots were developed using a chemiluminescence detection system (Amersham Bioscience, Piscataway, NJ).

Cytokine gene expression and protein secretion were analyzed using qRT-PCR and proteome profiler human angiogenesis array (R&D systems, Minneapolis, MN) according to the manufacturer's directions. After 2 weeks of coculture, cMSCs were sorted and plated to a 100 mm culture dish. Two days later, conditioned medium was collected for angiogenesis array, and RNA was extracted from the cells for qRT-PCR. To evaluate the paracrine molecule secretion activity of cMSCs after 1 week time point, 2 week cocultured cMSCs were sorted and plated to a 100 mm culture dish. One week later, the conditioned medium was collected for angiogenesis array. For the paracrine secretion activity characterization, the initial number of plated cells was kept the same for all groups (unmodified MSCs, MSCs cocultured with IONP(−)H9C2, cMSCs 2 days, and cMSCs 1 week). Quantitative analysis for angiogenesis array was performed with densitometry using ImageJ software from National Institutes of Health. The primers are listed in Supporting Information Table S1.

MI Model and Treatment. Myocardial infarction was induced in 8 week old Sprague−Dawley rats (240 ± 10 g) obtained from Samtako Bio (Osan, Korea), as previously described.[69] Briefly, after general anesthesia, the rat heart was exposed at the left costal rib through incision. Then, the left anterior descending artery (LAD) was ligated with a 6−0 silk suture (Ethicon, Cincinnati, OH) for 1 h and then reperfused. Infarction was macroscopically visualized as blanching in the left ventricle. For sham-operated Normal groups, no ligation was performed. For intramyocardial injection of MSCs and cMSCs, 1×10^6 cells were injected in a total volume of 60 μL of PBS using a 30-guage needle (BD Bioscience) 1 h after artery occlusion. Injections were made at the anterior and lateral aspects of the infarction border zone. For saline injection, 60 μL of saline was injected at the same sites. The use of animals was in accordance with the International Guide for the Care and Use of Laboratory Animals. The experimental protocol was approved by the Animal Research Committee of Yonsei University College of Medicine (IACUC No. 2012-0202-2).

Histological and Immunohistochemical Assessments. Two weeks after cell transplantation, the animals were sacrificed and the heart tissues were fixed with 10% (v/v) formaldehyde, embedded in paraffin, and sliced into 5 μm sections. To assess fibrotic tissue formation after infarction, the heart sections were stained with Masson's trichrome. The area of fibrotic tissue was measured using MetaMorph software (Molecular Devices, Sunnyvale, CA), and further expressed as the percentage to the total left ventricle.

To measure the infarct size of the myocardium, rat hearts were sectioned transaxially and incubated in TTC (Sigma) for 20 min under 37 °C, followed by 10% formalin fixation at 2−8 °C overnight. Infarcted region appeared yellow-white, and viable myocardium appeared red. Heart sections were photographed with a digital camera, and the area was measured with planimetry using ImageJ software. The area of infarction was expressed as the percentage of yellow-white infarct tissue to the total left ventricle.

Vessel density at peri-infarct was evaluated by staining tissue sections with anti-vWF antibody (Abcam) and anti-SMA-α antibody (Abcam). Fluorescent detection of vWF and SMA-α was visualized by FITC or Rhodamin-conjugated secondary antibody (Jackson ImmunoResearch Laboratories), respectively. Vessel structures positive for vWF or SMA-α expression were quantified for 4 animals per group, 2 slides per animal, and 3 to 4 fields per slide.

To evaluate tissue apoptosis, TUNEL (Chemicon, Billerica, MA) was used according to the manufacturer's instruction. The number of apoptotic cells was counted for 4 animals per group,

2 slides per animal, and 3 to 4 fields per slide. For the detection of Cx43 at the borderzone, anti-Cx43 antibody (Abcam) was used and detected with FITC-conjugated secondary antibody. Quantitative analysis was performed with densitometry using ImageJ software from National Institutes of Health.

Evaluation of Cardiac Functions. Two-dimensional transthoracic echocardiography was performed at baseline (normal) and for all experimental groups (n = 6 per group) 2 weeks after treatment. Assessments were carried out by an experienced cardiologist, blinded to the identity of the experimental groups. Images were acquired with a 14 MHz linear-array transducer interfaced with an ultrasound system (Vivid q, GE, Vigmed Ultrasound, Horten, Norway). Left ventricular internal diameters at end-systole (LVIDs) and at end-diastole (LVIDd) were measured from M-mode echocardiography in the midpapillary short axis view.

Conflict of Interest: The authors declare no competing financial interest.

Acknowledgment. This study was supported by the National Research Foundation of Korea (2013036054) and the Korea Health 21 R&D Project, Ministry of Health and Welfare (HI12C0199 and HI14C1550), Republic of Korea.

Supporting Information Available: Supplementary figures and tables. This material is available free of charge via the Internet at http://pubs.acs.org.

REFERENCES AND NOTES

1. Hatzistergos, K. E.; Quevedo, H.; Oskouei, B. N.; Hu, Q.; Feigenbaum, G. S.; Margitich, I. S.; Mazhari, R.; Boyle, A. J.; Zambrano, J. P.; Rodriguez, J. E.; et al. Bone Marrow Mesenchymal Stem Cells Stimulate Cardiac Stem Cell Proliferation and Differentiation. *Circ. Res.* **2010**, *107*, 913–922.
2. Nagaya, N.; Kangawa, K.; Itoh, T.; Iwase, T.; Murakami, S.; Miyahara, Y.; Fujii, T.; Uematsu, M.; Ohgushi, H.; Yamagishi, M.; et al. Transplantation of Mesenchymal Stem Cells Improves Cardiac Function in a Rat Model of Dilated Cardiomyopathy. *Circulation* **2005**, *112*, 1128–1135.
3. Williams, A. R.; Hare, J. M. Mesenchymal Stem Cells: Biology, Pathophysiology, Translational Findings, and Therapeutic Implications for Cardiac Disease. *Circ. Res.* **2011**, *109*, 923–940.
4. Quevedo, H. C.; Hatzistergos, K. E.; Oskouei, B. N.; Feigenbaum, G. S.; Rodriguez, J. E.; Valdes, D.; Pattany, P. M.; Zambrano, J. P.; Hu, Q.; McNiece, I.; et al. Allogeneic Mesenchymal Stem Cells Restore Cardiac Function in Chronic Ischemic Cardiomyopathy *via* Trilineage Differentiating Capacity. *Proc. Natl. Acad. Sci. U.S.A.* **2009**, *106*, 14022–14027.
5. Piao, H.; Youn, T. J.; Kwon, J. S.; Kim, Y. H.; Bae, J. W.; Bora, S.; Kim, D. W.; Cho, M. C.; Lee, M. M.; Park, Y. B. Effects of Bone Marrow Derived Mesenchymal Stem Cells Transplantation in Acutely Infarcting Myocardium. *Eur. J. Heart Failure* **2005**, *7*, 730–738.
6. Orlic, D.; Kajstura, J.; Chimenti, S.; Jakoniuk, I.; Anderson, S. M.; Li, B.; Pickel, J.; McKay, R.; Nadal-Ginard, B.; Bodine, D. M.; et al. Bone Marrow Cells Regenerate Infarcted Myocardium. *Nature* **2001**, *410*, 701–705.
7. Duran, J. M.; Makarewich, C. A.; Sharp, T. E.; Starosta, T.; Zhu, F.; Hoffman, N. E.; Chiba, Y.; Madesh, M.; Berretta, R. M.; Kubo, H.; et al. Bone-Derived Stem Cells Repair the Heart after Myocardial Infarction through Transdifferentiation and Paracrine Signaling Mechanisms. *Circ. Res.* **2013**, *113*, 539–552.
8. Mureli, S.; Gans, C. P.; Bare, D. J.; Geenen, D. L.; Kumar, N. M.; Banach, K. Mesenchymal Stem Cells Improve Cardiac Conduction by Upregulation of Connexin 43 through Paracrine Signaling. *Am. J. Physiol: Heart Circ. Physiol.* **2013**, *304*, H600–609.
9. Gnecchi, M.; He, H.; Liang, O. D.; Melo, L. G.; Morello, F.; Mu, H.; Noiseux, N.; Zhang, L.; Pratt, R. E.; Ingwall, J. S.; et al. Paracrine Action Accounts for Marked Protection of Ischemic Heart by Akt-Modified Mesenchymal Stem Cells. *Nat. Med.* **2005**, *11*, 367–368.
10. Mazhari, R.; Hare, J. M. Mechanisms of Action of Mesenchymal Stem Cells in Cardiac Repair: Potential Influences on the Cardiac Stem Cell Niche. *Nat. Clin. Pract. Cardiovasc. Med.* **2007**, *4* (Suppl 1), S21–26.
11. Gnecchi, M.; Zhang, Z.; Ni, A.; Dzau, V. J. Paracrine Mechanisms in Adult Stem Cell Signaling and Therapy. *Circ. Res.* **2008**, *103*, 1204–1219.
12. Roell, W.; Lewalter, T.; Sasse, P.; Tallini, Y. N.; Choi, B. R.; Breitbach, M.; Doran, R.; Becher, U. M.; Hwang, S. M.; Bostani, T.; et al. Engraftment of Connexin 43-Expressing Cells Prevents Post-Infarct Arrhythmia. *Nature* **2007**, *450*, 819–824.
13. Beeres, S. L.; Zeppenfeld, K.; Bax, J. J.; Dibbets-Schneider, P.; Stokkel, M. P.; Fibbe, W. E.; van der Wall, E. E.; Atsma, D. E.; Schalij, M. J. Electrophysiological and Arrhythmogenic Effects of Intramyocardial Bone Marrow Cell Injection in Patients with Chronic Ischemic Heart Disease. *Heart Rhythm* **2007**, *4*, 257–265.
14. Chen, H. S.; Kim, C.; Mercola, M. Electrophysiological Challenges of Cell-Based Myocardial Repair. *Circulation* **2009**, *120*, 2496–2508.
15. Chang, M. G.; Tung, L.; Sekar, R. B.; Chang, C. Y.; Cysyk, J.; Dong, P.; Marban, E.; Abraham, M. R. Proarrhythmic Potential of Mesenchymal Stem Cell Transplantation Revealed in an *In Vitro* Coculture Model. *Circulation* **2006**, *113*, 1832–1841.
16. Song, H.; Hwang, H. J.; Chang, W.; Song, B. W.; Cha, M. J.; Kim, I. K.; Lim, S.; Choi, E. J.; Ham, O.; Lee, C. Y.; et al. Cardiomyocytes from Phorbol Myristate Acetate-Activated Mesenchymal Stem Cells Restore Electromechanical Function in Infarcted Rat Hearts. *Proc. Natl. Acad. Sci. U.S.A.* **2011**, *108*, 296–301.
17. Hahn, J. Y.; Cho, H. J.; Kang, H. J.; Kim, T. S.; Kim, M. H.; Chung, J. H.; Bae, J. W.; Oh, B. H.; Park, Y. B.; Kim, H. S. Pre-Treatment of Mesenchymal Stem Cells with a Combination of Growth Factors Enhances Gap Junction Formation, Cytoprotective Effect on Cardiomyocytes, and Therapeutic Efficacy for Myocardial Infarction. *J. Am. Coll. Cardiol.* **2008**, *51*, 933–943.
18. Carvalho, J. L.; Braga, V.; Melo, M. B.; Campos, A. C. D.; Oliveira, M. S.; Gomes, D. A.; Ferreira, A. J.; Santos, R. A.; Goes, A. M. Priming Mesenchymal Stem Cells Boosts Stem Cell Therapy to Treat Myocardial Infarction. *J. Cell. Mol. Med.* **2013**, *17*, 617–625.
19. Ranganath, S. H.; Levy, O.; Inamdar, M. S.; Karp, J. M. Harnessing the Mesenchymal Stem Cell Secretome for the Treatment of Cardiovascular Disease. *Cell Stem Cell* **2012**, *10*, 244–258.
20. Ratajczak, M. Z.; Kucia, M.; Jadczyk, T.; Greco, N. J.; Wojakowski, W.; Tendera, M.; Ratajczak, J. Pivotal Role of Paracrine Effects in Stem Cell Therapies in Regenerative Medicine: Can We Translate Stem Cell-Secreted Paracrine Factors and Microvesicles into Better Therapeutic Strategies? *Leukemia* **2012**, *26*, 1166–1173.
21. Wen, Z.; Zheng, S.; Zhou, C.; Wang, J.; Wang, T. Repair Mechanisms of Bone Marrow Mesenchymal Stem Cells in Myocardial Infarction. *J. Cell. Mol. Med.* **2011**, *15*, 1032–1043.
22. Kinnaird, T.; Stabile, E.; Burnett, M. S.; Lee, C. W.; Barr, S.; Fuchs, S.; Epstein, S. E. Marrow-Derived Stromal Cells Express Genes Encoding a Broad Spectrum of Arteriogenic Cytokines and Promote *In Vitro* and *In Vivo* Arteriogenesis through Paracrine Mechanisms. *Circ. Res.* **2004**, *94*, 678–685.
23. Hwang, H. J.; Chang, W.; Song, B. W.; Song, H.; Cha, M. J.; Kim, I. K.; Lim, S.; Choi, E. J.; Ham, O.; Lee, S. Y.; et al. Antiarrhythmic Potential of Mesenchymal Stem Cell Is Modulated by Hypoxic Environment. *J. Am. Coll. Cardiol.* **2012**, *60*, 1698–1706.
24. Bhang, S. H.; Cho, S. W.; La, W. G.; Lee, T. J.; Yang, H. S.; Sun, A. Y.; Baek, S. H.; Rhie, J. W.; Kim, B. S. Angiogenesis in Ischemic Tissue Produced by Spheroid Grafting of Human Adipose-Derived Stromal Cells. *Biomaterials* **2011**, *32*, 2734–2747.

25. Mohanty, S.; Bose, S.; Jain, K. G.; Bhargava, B.; Airan, B. Tgfβ1 Contributes to Cardiomyogenic-Like Differentiation of Human Bone Marrow Mesenchymal Stem Cells. *Int. J. Cardiol.* **2011**, *163*, 93–99.
26. Antonitsis, P.; Ioannidou-Papagiannaki, E.; Kaidoglou, A.; Papakonstantinou, C. *In Vitro* Cardiomyogenic Differentiation of Adult Human Bone Marrow Mesenchymal Stem Cells. The Role of 5-Azacytidine. *Interact. Cardiovasc. Thorac. Surg.* **2007**, *6*, 593–597.
27. Makino, S.; Fukuda, K.; Miyoshi, S.; Konishi, F.; Kodama, H.; Pan, J.; Sano, M.; Takahashi, T.; Hori, S.; Abe, H.; et al. Cardiomyocytes Can Be Generated from Marrow Stromal Cells *In Vitro*. *J. Clin. Invest.* **1999**, *103*, 697–705.
28. Fukuhara, S.; Tomita, S.; Yamashiro, S.; Morisaki, T.; Yutani, C.; Kitamura, S.; Nakatani, T. Direct Cell-Cell Interaction of Cardiomyocytes Is Key for Bone Marrow Stromal Cells to Go into Cardiac Lineage *In Vitro*. *J. Thorac. Cardiovasc. Surg.* **2003**, *125*, 1470–1480.
29. Murasawa, S.; Kawamoto, A.; Horii, M.; Nakamori, S.; Asahara, T. Niche-Dependent Translineage Commitment of Endothelial Progenitor Cells, Not Cell Fusion in General, into Myocardial Lineage Cells. *Arterioscler., Thromb., Vasc., Biol.* **2005**, *25*, 1388–1394.
30. Cselenyák, A.; Pankotai, E.; Horváth, E. M.; Kiss, L.; Lacza, Z. Mesenchymal Stem Cells Rescue Cardiomyoblasts from Cell Death in an *In Vitro* Ischemia Model *via* Direct Cell-to-Cell Connections. *BMC Cell Biol.* **2010**, *11*, 29.
31. Song, D.; Liu, X.; Liu, R.; Yang, L.; Zuo, J.; Liu, W. Connexin 43 Hemichannel Regulates H9C2 Cell Proliferation by Modulating Intracellular Atp and [Ca2+]. *Acta Biochim. Biophys. Sin.* **2010**, *42*, 472–482.
32. Connell, J. P.; Augustini, E.; Moise, K. J., Jr.; Johnson, A.; Jacot, J. G. Formation of Functional Gap Junctions in Amniotic Fluid-Derived Stem Cells Induced by Transmembrane Co-Culture with Neonatal Rat Cardiomyocytes. *J. Cell. Mol. Med.* **2013**, *17*, 774–781.
33. Hachani, R.; Lowdell, M.; Birchall, M.; Thanh, N. T. Tracking Stem Cells in Tissue-Engineered Organs Using Magnetic Nanoparticles. *Nanoscale* **2013**, *5*, 11362–11373.
34. Chertok, B.; Moffat, B. A.; David, A. E.; Yu, F.; Bergemann, C.; Ross, B. D.; Yang, V. C. Iron Oxide Nanoparticles as a Drug Delivery Vehicle for MRI Monitored Magnetic Targeting of Brain Tumors. *Biomaterials* **2008**, *29*, 487–496.
35. Kim, J. A.; Lee, N.; Kim, B. H.; Rhee, W. J.; Yoon, S.; Hyeon, T.; Park, T. H. Enhancement of Neurite Outgrowth in PC12 Cells by Iron Oxide Nanoparticles. *Biomaterials* **2011**, *32*, 2871–2877.
36. Chen, Y. C.; Hsiao, J. K.; Liu, H. M.; Lai, I. Y.; Yao, M.; Hsu, S. C.; Ko, B. S.; Chen, Y. C.; Yang, C. S.; Huang, D. M. The Inhibitory Effect of Superparamagnetic Iron Oxide Nanoparticle (Ferucarbotran) on Osteogenic Differentiation and Its Signaling Mechanism in Human Mesenchymal Stem Cells. *Toxicol. Appl. Pharmacol.* **2010**, *245*, 272–279.
37. Huang, X.; Zhang, F.; Wang, Y.; Sun, X.; Choi, K. Y.; Liu, D.; Choi, J. S.; Shin, T. H.; Cheon, J.; Niu, G.; et al. Design Considerations of Iron-Based Nanoclusters for Noninvasive Tracking of Mesenchymal Stem Cell Homing. *ACS Nano* **2014**, *8*, 4403–4414.
38. Lee, N.; Choi, Y.; Lee, Y.; Park, M.; Moon, W. K.; Choi, S. H.; Hyeon, T. Water-Dispersible Ferrimagnetic Iron Oxide Nanocubes with Extremely High R(2) Relaxivity for Highly Sensitive *In Vivo* MRI of Tumors. *Nano Lett.* **2012**, *12*, 3127–3131.
39. Singh, N.; Jenkins, G. J.; Asadi, R.; Doak, S. H. Potential Toxicity of Superparamagnetic Iron Oxide Nanoparticles (SPION). *Nano Rev.* **2010**, *1*, 5358.
40. Turk, M. J.; Reddy, J. A.; Chmielewski, J. A.; Low, P. S. Characterization of a Novel pH-Sensitive Peptide That Enhances Drug Release from Folate-Targeted Liposomes at Endosomal pHs. *Biochim. Biophys. Acta* **2002**, *1559*, 56–68.
41. Li, K.; Chi, Y.; Gao, K.; Yan, Q.; Matsue, H.; Takeda, M.; Kitamura, M.; Yao, J. Connexin43 Hemichannel-Mediated Regulation of Connexin43. *PLoS One* **2013**, *8*, e58057.
42. Sato, D.; Xie, L. H.; Sovari, A. A.; Tran, D. X.; Morita, N.; Xie, F.; Karagueuzian, H.; Garfinkel, A.; Weiss, J. N.; Qu, Z. Synchronization of Chaotic Early Afterdepolarizations in the Genesis of Cardiac Arrhythmias. *Proc. Natl. Acad. Sci. U.S.A.* **2009**, *106*, 2983–2988.
43. De Bakker, J.; Van Capelle, F.; Janse, M. J.; Tasseron, S.; Vermeulen, J. T.; De Jonge, N.; Lahpor, J. R. Slow Conduction in the Infarcted Human Heart.'Zigzag'course of Activation. *Circulation* **1993**, *88*, 915–926.
44. Zhang, H.; Yuan, X.; Jin, P. F.; Hou, J. F.; Wang, W.; Wei, Y. J.; Hu, S. Alteration of Parasympathetic/Sympathetic Ratio in the Infarcted Myocardium after Schwann Cell Transplantation Modified Electrophysiological Function of Heart: A Novel Antiarrhythmic Therapy. *Circulation* **2010**, *122*, S193–200.
45. Nattel, S.; Maguy, A.; Le Bouter, S.; Yeh, Y. H. Arrhythmogenic Ion-Channel Remodeling in the Heart: Heart Failure, Myocardial Infarction, and Atrial Fibrillation. *Physiol. Rev.* **2007**, *87*, 425–456.
46. Reinecke, H.; Minami, E.; Virag, J. I.; Murry, C. E. Gene Transfer of Connexin43 into Skeletal Muscle. *Hum. Gene Ther.* **2004**, *15*, 627–636.
47. He, X. Q.; Chen, M. S.; Li, S. H.; Liu, S. M.; Zhong, Y.; McDonald Kinkaid, H. Y.; Lu, W. Y.; Weisel, R. D.; Li, R. K. Co-Culture with Cardiomyocytes Enhanced the Myogenic Conversion of Mesenchymal Stromal Cells in a Dose-Dependent Manner. *Mol. Cell. Biochem.* **2010**, *339*, 89–98.
48. Plotnikov, E.; Khryapenkova, T.; Vasileva, A.; Marey, M.; Galkina, S.; Isaev, N.; Sheval, E.; Polyakov, V.; Sukhikh, G.; Zorov, D. Cell-to-Cell Cross-Talk between Mesenchymal Stem Cells and Cardiomyocytes in Co-Culture. *J. Cell. Mol. Med.* **2008**, *12*, 1622–1631.
49. Takahashi, K.; Ito, Y.; Morikawa, M.; Kobune, M.; Huang, J.; Tsukamoto, M.; Sasaki, K.; Nakamura, K.; Dehari, H.; Ikeda, K.; et al. Adenoviral-Delivered Angiopoietin-1 Reduces the Infarction and Attenuates the Progression of Cardiac Dysfunction in the Rat Model of Acute Myocardial Infarction. *Mol. Ther.* **2003**, *8*, 584–592.
50. Zhou, L.; Ma, W.; Yang, Z.; Zhang, F.; Lu, L.; Ding, Z.; Ding, B.; Ha, T.; Gao, X.; Li, C. Vegf165 and Angiopoietin-1 Decreased Myocardium Infarct Size through Phosphatidylinositol-3 Kinase and Bcl-2 Pathways. *Gene Ther.* **2005**, *12*, 196–202.
51. Stavropoulou, A.; Philippou, A.; Halapas, A.; Sourla, A.; Pissimissis, N.; Koutsilieris, M. Upa, Upar and Tgfbeta(1) Expression During Early and Late Post Myocardial Infarction Period in Rat Myocardium. *In Vivo* **2010**, *24*, 647–652.
52. Kinnaird, T.; Stabile, E.; Burnett, M. S.; Shou, M.; Lee, C. W.; Barr, S.; Fuchs, S.; Epstein, S. E. Local Delivery of Marrow-Derived Stromal Cells Augments Collateral Perfusion through Paracrine Mechanisms. *Circulation* **2004**, *109*, 1543–1549.
53. Isogai, C.; Laug, W. E.; Shimada, H.; Declerck, P. J.; Stins, M. F.; Durden, D. L.; Erdreich-Epstein, A.; DeClerck, Y. A. Plasminogen Activator Inhibitor-1 Promotes Angiogenesis by Stimulating Endothelial Cell Migration toward Fibronectin. *Cancer Res.* **2001**, *61*, 5587–5594.
54. Zaman, A. K.; Fujii, S.; Schneider, D. J.; Taatjes, D. J.; Lijnen, H. R.; Sobel, B. E. Deleterious Effects of Lack of Cardiac PAI-1 after Coronary Occlusion in Mice and Their Pathophysiologic Determinants. *Histochem. Cell Biol.* **2007**, *128*, 135–145.
55. Rychli, K.; Huber, K.; Wojta, J. Pigment Epithelium-Derived Factor (PEDF) as a Therapeutic Target in Cardiovascular Disease. *Expert Opin. Ther. Targets* **2009**, *13*, 1295–1302.
56. Rosano, J. M.; Cheheltani, R.; Wang, B.; Vora, H.; Kiani, M. F.; Crabbe, D. L. Targeted Delivery of Vegf after a Myocardial Infarction Reduces Collagen Deposition and Improves Cardiac Function. *Cardiovasc. Eng. Technol.* **2012**, *3*, 237–247.
57. Ellison, G. M.; Nadal-Ginard, B.; Torella, D. Optimizing Cardiac Repair and Regeneration through Activation of the Endogenous Cardiac Stem Cell Compartment. *J. Cardiovasc. Transl. Res.* **2012**, *5*, 667–677.
58. Trivedi, P.; Tray, N.; Nguyen, T.; Nigam, N.; Gallicano, G. I.; Mesenchymal Stem, Cell Therapy for Treatment of Cardiovascular Disease: Helping People Sooner or Later. *Stem Cells Dev.* **2010**, *19*, 1109–1120.

59. Dai, W.; Hale, S. L.; Martin, B. J.; Kuang, J. Q.; Dow, J. S.; Wold, L. E.; Kloner, R. A. Allogeneic Mesenchymal Stem Cell Transplantation in Postinfarcted Rat Myocardium: Short- and Long-Term Effects. *Circulation* **2005**, *112*, 214–223.
60. Henkel, D. M.; Witt, B. J.; Gersh, B. J.; Jacobsen, S. J.; Weston, S. A.; Meverden, R. A.; Roger, V. L. Ventricular Arrhythmias after Acute Myocardial Infarction: A 20-Year Community Study. *Am. Heart J.* **2006**, *151*, 806–812.
61. Deuse, T.; Peter, C.; Fedak, P. W.; Doyle, T.; Reichenspurner, H.; Zimmermann, W. H.; Eschenhagen, T.; Stein, W.; Wu, J. C.; Robbins, R. C.; et al. Hepatocyte Growth Factor or Vascular Endothelial Growth Factor Gene Transfer Maximizes Mesenchymal Stem Cell-Based Myocardial Salvage after Acute Myocardial Infarction. *Circulation* **2009**, *120*, S247–254.
62. Noiseux, N.; Gnecchi, M.; Lopez-Ilasaca, M.; Zhang, L.; Solomon, S. D.; Deb, A.; Dzau, V. J.; Pratt, R. E. Mesenchymal Stem Cells Overexpressing Akt Dramatically Repair Infarcted Myocardium and Improve Cardiac Function Despite Infrequent Cellular Fusion or Differentiation. *Mol. Ther.* **2004**, *14*, 840–850.
63. Iso, Y.; Spees, J. L.; Serrano, C.; Bakondi, B.; Pochampally, R.; Song, Y.-H.; Sobel, B. E.; Delafontaine, P.; Prockop, D. J. Multipotent Human Stromal Cells Improve Cardiac Function after Myocardial Infarction in Mice without Long-Term Engraftment. *Biochem. Biophys. Res. Commun.* **2007**, *354*, 700–706.
64. Wang, X.; Jameel, M. N.; Li, Q.; Mansoor, A.; Qiang, X.; Swingen, C.; Panetta, C.; Zhang, J. Stem Cells for Myocardial Repair with Use of a Transarterial Catheter. *Circulation* **2009**, *120*, S238–S246.
65. Mazo, M.; Gavira, J. J.; Abizanda, G.; Moreno, C.; Ecay, M.; Soriano, M.; Aranda, P.; Collantes, M.; Alegría, E.; Merino, J. Transplantation of Mesenchymal Stem Cells Exerts a Greater Long-Term Effect Than Bone Marrow Mononuclear Cells in a Chronic Myocardial Infarction Model in Rat. *Cell Transplant.* **2010**, *19*, 313–328.
66. Mazo, M.; Planat-Bénard, V.; Abizanda, G.; Pelacho, B.; Léobon, B.; Gavira, J. J.; Peñuelas, I.; Cemborain, A.; Pénicaud, L.; Laharrague, P. Transplantation of Adipose Derived Stromal Cells Is Associated with Functional Improvement in a Rat Model of Chronic Myocardial Infarction. *Eur. J. Heart Failure* **2008**, *10*, 454–462.
67. Tang, Y. L.; Tang, Y.; Zhang, Y. C.; Qian, K.; Shen, L.; Phillips, M. I. Improved Graft Mesenchymal Stem Cell Survival in Ischemic Heart with a Hypoxia-Regulated Heme Oxygenase-1 Vector. *J. Am. Coll. Cardiol.* **2005**, *46*, 1339–1350.
68. Li, Z.; Guo, J.; Chang, Q.; Zhang, A. Paracrine Role for Mesenchymal Stem Cells in Acute Myocardial Infarction. *Biol. Pharm. Bull.* **2009**, *32*, 1343–1346.
69. Kim, S. H.; Moon, H. H.; Kim, H. A.; Hwang, K. C.; Lee, M.; Choi, D. Hypoxia-Inducible Vascular Endothelial Growth Factor-Engineered Mesenchymal Stem Cells Prevent Myocardial Ischemic Injury. *Mol. Ther.* **2011**, *19*, 741–750.